RSC Advances

ROYAL SOCIETY OF CHEMISTRY

www.rsc.org/advances

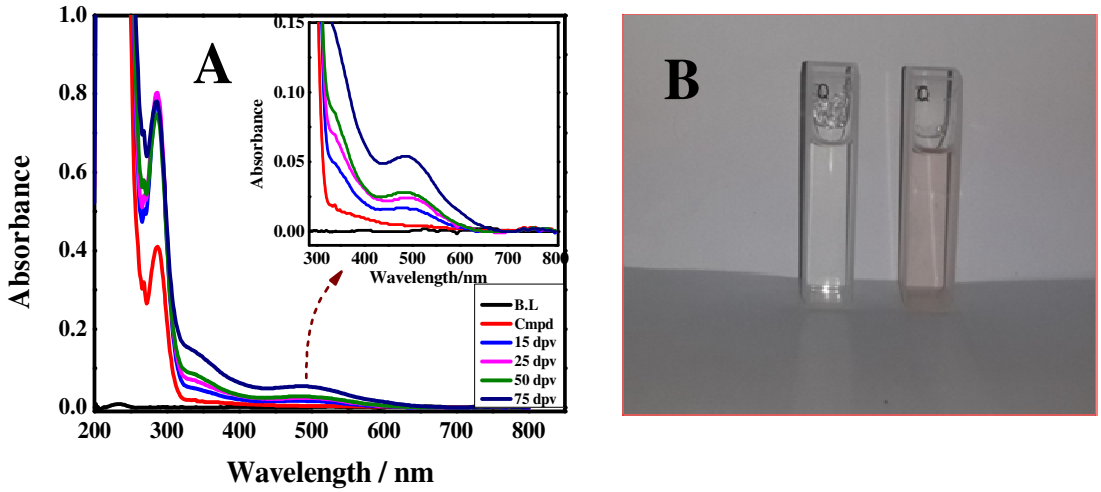

The electrochemical oxidation of anilines resulted in azodye formation which was evidenced by the appearance of a new peak in the UV-visible spectra (A) and colour change of solution (B).

pH and Temperature Responsive Redox Behavior of Biologically Important Aniline Derivatives

Hanif Subhan[a], Aref Lashin[b,c], Usman Ali Rana[d], Nassir Al-Arifi[e], Khurshid Ahmad[a], Hidayat Hussain[f], Rumana Qureshi[a], Saqib Ali[a], Muhammad Abid Zia[g], Heinz-Bernhard Kraatz[h] and Afzal Shah[a,h*]

[a]Department of Chemistry, Quaid-i-Azam University, 45320, Islamabad, Pakistan

[b]King Saud University, College of Engineering - Petroleum and Gas Engineering Department, P.O. Box 800, Riyadh 11421 - Saudi Arabia.

[c]Benha University, Faculty of Science - Geology Department, P.O. Box 13518, Benha- Egypt.

[d]Sustainable Energy Technologies Center, PO-box-800, King Saud University, Riyadh 11421, Saudi Arabia

[e]King Saud University, College of Science - Geology and Geophysics Department, P.O. Box 2455, Riyadh 11451 - Saudi Arabia.

[f]UoN Chair of Oman's Medicinal Plants and Marine Natural Products, University of Nizwa, Birkat Al-Mauz, Nizwa 616, Oman

[g]University of Education, Attock campus Attock

[h]Department of Physical and Environmental Sciences, University of Toronto Scarborough, 1265 Military Trail, Toronto, M1C 1A4, Canada

*To whom correspondence should be addressed

Dr Afzal Shah

Tel: +92-5190642110

E-mail: afzals_qau@yahoo.com and afzal.shah@utoronto.ca

Abstract

The redox behavior of two biologically important aniline derivatives, 2-(4-aminophenyl) ethanol and 4-aminobenzoic acid was scrutinized in a wide pH range of 2.0-12.0 using modern electrochemical techniques. The results of cyclic voltammetric experiments conducted at different temperatures were used for the evaluation of kinetic and thermodynamic parameters such as diffusion coefficient, heterogeneous electron transfer rate constant, Gibbs free energy, enthalpy and entropy changes. Differential pulse voltammetry was employed for the determination of acid-base dissociation constant (pKa) and evaluation of number of electrons and protons involved in redox reactions. The comparatively more rapid and sensitive voltammetric technique, square wave voltammetry allowed the determination of quite lower limit of detection and quantification of the analytes. Computational studies were performed for the identification of the most favorable oxidizable electropores of the compounds and for developing structure-activity relationships in conjunction with the experimental results. On the basis of electrochemical and computational findings a comprehensive redox mechanism was proposed which may provide useful insights about the role by which this class of compounds exert their biological action. The proposed mechanism was found in line with the analysis of the product scratched from the electrode surface.

Key words: Redox behavior; pH responsiveness; Kinetics; Thermodynamics; Computational studies.

1. Introduction

In spite of the fact that aniline is toxic, a plethora of its derivatives possess potent anticancer[1-3] anti-HIV,[4] antioxidant,[5-7] antifungal[8] and antimicrobial activities.[9] Aniline mustards have been reported to exhibit significant antitumor properties and two representatives (chlorambucil and melphalan) of this class have achieved clinical status for cancer treatment[1]. Likewise, aniline containing sorafenib and its derivatives are promising antitumor agents.[10] Homoallylamines possess good antifungal activities.[11] Similarly, the antifungal properties of hetaryl groups bearing substituted anilines have been reported.[12] Thiourea derivatives containing aniline moiety have also been documented as potent antibacterial agents[13]. A survey of recent literature reveals that electron transfer reactions are responsible for the biological activities of aniline derivatives.[14] Consequently, detailed knowledge about the redox behavior of this class seems conceivable for comprehending the mechanism of their biological action. Literature survey reveals that extensive information is available about the use of anilines as redox probes and electron transfer mediators.[15-18] However, meager information about the pH dependent electron transfer reactions of anilines and no information about the thermodynamics of their proton coupled electron transfer processes are available in literature. Thus, the current work is an effort for the partial fulfilment of this gap in literature.

In agriculture, a range of aniline based compounds are used as chemical weapons for eradicating the undesirable plants. Sulphonylureas, phenylureas and chloroacetanilides represent important families of aniline based herbicides which have registered their potency on commercial scale.[19,20] These herbicides exert their action either by diverting the flow of electron in photosynthesis from its normal pathway or inhibit acetolactose-synthatase enzyme.[19,21] Therefore, our current investigations about the redox mechanistic pathways of

aniline derivatives are expected to provide some useful guidelines for facilitating prediction of herbicidal role of this class of compounds.

Polyaniline is the most extensively studied ionic conducting polymers due to its high conductivity, robust electrochemistry and electrochromic effects. Polyanilines find extensive applications in rechargeable batteries,[22] microelectronics[23] and electrochromic display devices.[24] Moreover, polyanilines of high water solubility are developed for lithography and mass inspection in scanning electron microscopy.[25] Changes in conditions such as temperature and pH of the medium can have a remarkable influence on the course of electron transfer reactions. Thus, spurred on by the broad range applications of aniline derivatives, we probed the pH and temperature responsive redox mechanism of two unexplored representatives of this class by electrochemical techniques and computational studies. The previous investigators have reported that oxidation of anilines leads to the formation of azo dyes which can act as electro-optical sensors.[26] Interestingly, the results of our experiments also show that the oxidation product of anilines is both electroactive and photoactive. We have experimentally confirmed the final product of the proposed redox mechanism and thus, the current work is expected to be a valuable addition to the literature of aniline derivatives.

2. Experimental

2.1. Chemicals and reagents

Analytical grade 4-aminophenyl alcohol (4-APA) and 4-aminobenzoic acid (4-ABA) were obtained from sigma Aldrich and used as received. Stock solutions of 2.0 mM concentration were prepared in ethanol and stored at 4 ^{o}C. Fresh solutions in buffer and ethanol (1:1) mixture were prepared from stock solutions for experimental work. Britton–Robinson (BR) buffer of 0.2 M ionic strength in the pH rang 2.0-12.0 was employed as supporting

electrolyte. Bidistilled water of ≤0.1 μS /cm conductance was used for the preparation of BR-buffer solutions.

2.2. Equipments and measurements

All voltammetric experiments were performed using μAutolab running with GPES 4.9 software Eco-Chemie, The Netherlands. Glassy carbon (GC) having surface area of 0.071cm^2 was employed as working electrode while Pt-wire was used as counter electrode. Besides this, Ag/AgCl electrode consisting of 3 M KCL solution was used as reference electrode. Before recording any voltammetric scan, the dissolved oxygen was flushed out by purging argon for 10 minutes and the surface of GCE was polished with diamond spray (having particle size of 1 μm) followed by thorough rising with a jet of doubly distilled water. The reproducibility of experimental results was ensured by placing the polished electrode in the buffer electrolyte of desired pH followed by recording various voltammograms up to the attainment of a steady state base line. For differential pulse voltammetry, pulse amplitude of 50 mV and pulse width of 70 ms were set as experimental conditions. Similarly for square wave voltammetry (SWV), the experimental conditions were 2 mV potential increments and 50 Hz frequency with an effective sweep rate of 100 mVs^{-1}. Temperature was kept constant by immersing the measurement cell in a water circulating bath (IRMECO I-2400 GmbH Germany). Gaussian 03 package was used for computational studies. The geometric structures were first optimized at hybrid Becke three- parameter Lee–Yang–Parr exchange correlation functional (B3LYP) level of 631-G basis set and then the most stable conformations were proceeded for charge distribution calculation.

3. Results and Discussion

3.1. Cyclic Voltammetry (CV)

CV was used for getting a general portrait of the redox behavior of the compounds. CVs of 4-APA and 4-ABA shown in **Fig. 1** depict a prominent and well defined anodic wave, 1a, at 0.79 and 0.82 V respectively. The appearance of a very small cathodic peak corresponding to the reduction of the oxidized product of 1a in the reverse scan demonstrates the quasi-reversible nature of the inclusive oxidation process. The different current intensities (Ia/Ic ≠ 1) of the anodic and cathodic signals point to follow up reactions of the oxidized product. The broad reduction signals of 4-APA and 4-ABA at -0.64 and -0.62 V disappear after purging with argon and hence these emerge due to reduction of interrupting dissolved oxygen. Besides the above mentioned signals, 4-ABA also shows a reduction wave, 1c*, at -0.10 V with corresponding oxidation signal (2a) at -0.03 V in the next successive scan. The peak separation of 49 mV demonstrates the reversible nature of the redox couple labeled as 2a and 1c. Moreover, the comparatively lower oxidation potential of 4-APA suggests this compound as a comparatively stronger reducing agent than 4-ABA. The rationale behind the lower oxidation potential of 4-APA can be related to the electron donating effect (via hyper conjugation) of the alkyl group to encourage the oxidation of amino group as compared to 4-ABA possessing COOH as electron withdrawing group at the aromatic ring.

The effect of sweep rate variation on the CV response of the analytes was examined in a medium of pH 7.4 for the determination of diffusion coefficient (*D*) at different temperatures. The CVs shown in **Fig. S1** demonstrate the intensification of the peak current with rise in temperature due to possible decrease in the viscosity of solution. Moreover, the peak exhibits a slight shift with rise in temperature and sweep rate, thus, suggesting the quasi-reversible nature of the electrochemical oxidation.[27] The *D* values of the analytes were

evaluated at different temperatures from the slopes of the linear plots (**Fig. 2**) of peak current (I_p) vs square root of scan rate ($\upsilon^{1/2}$) using Randles-Sevcik equation.[28]

$$I_p = \frac{5.16 \times 10^6 n(\alpha_a n)^{1/2} ACD^{1/2} \nu^{1/2}}{T^{1/2}} \qquad 3.1$$

Where n denotes the number of electrons involved in oxidation reaction, α_a the anodic charge transfer coefficient, A the area of electrode (cm^2), *D* the diffusivity constant (cm/s) and C the bulk concentration (mol/cm^3) of analyte. The $\alpha_a n$ values listed in **Table 1** were evaluated from the difference of E_p and $E_{p/2}$ of the cyclic voltammetric signals shown in **Fig. S1** using the equation, $E_p - Ep_{/2} = \frac{0.0477}{\alpha_a n}$. Inspection of table 1 reveals that the value of *D* progressively increases with rise in temperature because of lower solution resistance due to increase in kinetic energy of the species at higher temperature. The *D* value of 4-APA is greater than 4-ABA due to comparatively lower molecular mass and less polar nature (thus experiencing lesser attraction with the solvent) as evidenced by its computationally determined smaller dipole moment (vide infra in table 5). The linear log plots of peak current *versus* sweep rate shown in **Fig. S2** having slope values quite close to the theoretical value of 0.5 point to the diffusion controlled nature of the oxidation processes of 4-APA and 4-ABA according to the criteria reported by the previous investigators.[29-31] The value of heterogeneous electron transfer rate constant (*k*), an imperative parameter for predicting the nature of redox process was calculated on the basis of peak 1a at different temperatures using the equation reported in literature.[32] An examination of table 1 and Fig. S1 reveals that the oxidation potential drifts towards lower potentials and the values of *k* increase with rise in temperature thus, signifying the facile electron abstraction at higher temperature.

$$I_{pa}/nFAC = k \qquad 3.2$$

Where n, A, F and *k* represent number of electrons, active surface of working electrode, Faraday's constant and heterogeneous electron transfer rate constant.

For getting insights about the thermodynamics of the electrode processes, some valuable thermodynamic parameters such as Gibbs free energy (ΔG), enthalpy (ΔH) and entropy changes (ΔS) were determined. The values of *k* calculated at five different temperature values were subsequently employed for ΔG determination by using the following equation.[33]

$$\Delta G = 5778.8(5.096 - \log k) \quad 3.3$$

The slope of the Arrhenius plots shown in **Fig. 3** were used for the determination of activation energy (E_a). Enthalpy and entropy changes were then determined according to the following equations.[33]

$$\Delta H = E_a - RT \quad 3.4$$

$$\Delta G = \Delta H - T\Delta S \quad 3.5$$

Thermodynamic parameters listed in **Table 2** show positive values of ΔG and ΔH thus, demonstrating the non-spontaneous and endothermic nature of the oxidation process while negative ΔS points to entropy opposed process. Negative ΔS means that the product has lower entropy than the reactant, hence, the ordered nature of the oxidized product can be related to its adsorption over the electrode surface. Furthermore, the gradual decrease in ΔG with temperature rise shows the inclination of redox reaction towards reversibility. In contrast, the increase in ΔS values with elevation of temperature indicate increase of randomness in the system as expected.

3.2. Differential pulse voltammetry (DPV)

The redox behaviour of aniline derivatives was also probed by DPV, as this technique has the ability of minimizing the charging current and extracting Faradaic current which leads to enhanced sensitivity and greater accuracy.[34] The DPVs of 4-APA depicted in **Fig. 4A** shows two small peaks 2a and 3a besides the main oxidation signal in acidic media while no such signals can be seen in the DPVs of 4-ABA (**Fig. 5A**). The peak potentials of both compounds shift cathodically with increasing pH of the medium indicating facile electron abstraction under higher pH conditions. The half peak width ($W_{1/2}$) values calculated according to equation 3.6,[35] show one electron transfer during oxidation of the selected aniline derivatives. The number of protons accompanying the electron transfer reactions was determined from equation 3.7. Below pH 6, the slope of E_p-pH plot corresponding to peak 1a is 21 mV per pH unit which indicates the loss of 0.14 proton and one electron from a single molecule of 4-APA. This suggests the loss of one proton and seven electrons from seven molecules of 4-APA in acidic conditions of pH $\leq$ 6. The slope of 37 mV per pH unit in neutral and alkaline conditions reveals the oxidation by the involvement of 0.25 protons and one electron per single molecule of 4-APA. Thus, the oxidation of 4 molecules of 4-APA occurs by the abstraction of $1H^+$ and 4e. The E_p *versus* pH plot of 4-APA (**Fig. 4B)** shows the switching of mechanism at pH around 6.0 and this behavior is in good agreement with the reported results of structurally related compounds.[36,37] Similar calculations for peaks 2a and 3a of 4-APA indicate the participation of protons during electron transfer reactions (**Fig. 4C**). In case of 4-ABA, the involvement of three electrons and one proton per three molecules is suggested in the light of DPV results obtained in media of pH less than 7.9. In media of pH higher than this value, protons involvement is not evidenced during electron transfer reactions (**Fig. 5B)**. The parameters obtained from DPVs can be seen in **Table 3.**

$$W_{1/2} = 90.4 / \alpha n_a \qquad 3.6$$

No. of protons= (dE/dpH) (αn_a)/ 0.059 3.7

3.3. Square wave voltammetry (SWV)

Due to the associated advantages of detecting lower concentration of the analytes, higher sensitivity and rapid pace of analysis,[38] SWV was employed for the determination of the limit of detection (LOD) and the limit of quantification (LOQ) of aniline derivatives. The peak current of the calibration standards regularly increase with rise in concentration of the substrate as expected (**Fig. 6**). Nicely linear calibration plots in the concentration range of 30 μM to 0.4 mM and 7.5 μM to 0.11mM were obtained for 4- APA and 4-ABA (see inset of **Fig.6**). The slope values of the linear range of the calibration curves were used for the calculation of LOD and LOQ using equations 3.8 and 3.9.[39]

LOD = 3SD / m 3.8

LOQ = 10SD / m 3.9

Where SD stands for the standard deviation of intercept and m represents slope of the linear segment of I_p plotted against concentration.

The LOD and LOQ of both compounds and the regression parameters of the calibration curve are listed in **Table 4.** The obtained detection values clearly indicate that very low concentrations of the selected aniline derivatives can be detected using square wave voltammetric method. The detection limits are comparable with the reported values of structurally related aniline derivatives.

3.4. Computational studies

Computational studies were carried for the identification of the most favorable oxidizable moiety in the compounds. First, the geometry of the compounds was optimized followed by Mullikan charge densities calculation using standard 6-31-G basis set in Gaussian-3 package.

Both aniline derivatives exhibited the highest negative charge on nitrogen atom of NH_2 group, suggesting it as the most favorable centre for electrochemical oxidation as shown in **Fig. 7**. Moreover, the less negative energy of the highest occupied molecular orbital (E_{HOMO}) of 4-APA than 4-ABA demonstrate its easier oxidation thus, supporting cyclic voltammetric results. We used computational chemistry for the determination of E_{LUMO}, ionization energy, electron affinity and dipole moment (**Table 5)** of the compounds. These parameters helped in offering explanation to the voltammetric observations; for instance, the smaller *D* of 4-ABA than 4-APA was explained on the basis of its higher dipole moment. So, the more polar 4-ABA will experience greater friction thus, hindering its mobility towards the electrode surface.

3.5. Redox mechanism of aniline derivatives

In the light of computational findings and experimental results obtained from the three electrochemical techniques, pH dependent redox mechanisms were suggested. Both the compounds displayed a prominent and stable oxidation peak, 1a, in all the studied pH conditions (**Fig. 1A**). Based on recent literature survey and computational investigations, it is proposed that signal 1a emerges due to oxidation of -NH_2 group of the compounds.[40] The width at half peak height of peak 1a represents the loss of one electron from this moiety. The slope of E_p-pH plot corresponding to peak 1a indicates the accompaniment of only 0.14 proton during an electron transfer reaction of 4-APA. Thus, based upon the quasi-reversible oxidation as evidenced by cyclic voltammetric result of $I_a/I_c \neq 1$ and literature report,[41] the molecule of 4-APA is suggested to form a cationic radical followed by the formation of a free radical through chemical deprotonation as shown in **Scheme 1**. In the next step two free radicals may combine thus leading to the formation of a stable dimer. The two small anodic signals, 2a and 3a, in 4-APA are ascribed to successive one electron and one proton loss from the dimer resulting in the formation of a stable azodye. The formation of such dyes has also

been reported by the previous researchers for compounds structurally related to 4-APA.[40, 42] In solutions of pH higher than 6.0, only the main oxidation signal 1a was registered in the voltammograms. From the $W_{1/2}$ values and slope of the plot between E_p and pH, the redox mechanism shown in **Scheme 2** was suggested. The proposed oxidation mechanism of 4-ABA is presented in **Scheme 3**.

Confirmation of the product (Azo dye): Electronic absorption spectroscopy and color response of the solution provided clues about the formation of azo dye. The UV-Vis spectrum of 4-APA showed no signal at 485 nm but the spectra of the product scratched from the electrode surface after recording multiple differential pulse voltammograms indicated an increase in absorbance that finally developed into a noticeable band around this wavelength region as shown in **Fig. 8A**. The color response of the solution also offered evidence about the formation of azo-dye. The solution of the starting compound is colorless but the solution of the product scratched from the electrode surface after 75 DPV scans appears light red **(Fig. 8B).** The azo dye possesses -N=N-chromophore which gives a well-defined signal in the visible region as documented by some investigators.[43,44]

4. Conclusion

Both the aniline derivatives 4-aminophenyl alcohol (4-APA) and 4-aminobenzoic acid (4-ABA) exhibited pH dependent and diffusion controlled quasi-reversible mode of oxidation at GC-electrode. The appearance of corresponding small cathodic signals and values of heterogeneous electron transfer rate constant suggested the quasi-reversible nature of the redox processes. Temperature effect monitored for thermodynamic assessment of the electron transfer reactions indicated non-spontaneous, endothermic and entropy opposed nature of the oxidation processes. The increase in diffusion coefficient with rising temperature can be

related to the decrease in viscosity and concomitant increase in kinetic energy of the molecules. Likewise, the value of heterogeneous rate constant increased with elevation in temperature leading the redox process to incline towards reversibility. Moreover, the lowering of $\Delta G^{\#}$ and increasing of $\Delta S^{\#}$ values with rise in temperature reveals the drift of oxidation process towards spontaneity and increase in degree of disorder of the resulting product. Unlike the analytes, their oxidized products were found to show reversible redox behavior as evidenced by the appearance of signals corresponding to a reversible redox couple. The redox mechanistic pathways of the selected anilines were proposed on the basis of experimental and computational findings. Interestingly the analysis of the product formed at the electrode surface supported the suggested mechanism.

Acknowledgments

The authors are thankful to Higher Education Commission and Quaid-i-Azam University, Islamabad, Pakistan. The authors also extend their sincere appreciations to the Deanship of Scientific Research at the King Saud University for its funding this Prolific Research Group (PRG-1436-08).

References

1 A. Prakash, W.A. Denny, T.A. Gourdie, K.K. Valu, P.D. Woodgate and L.P. Wakelin, *Biochemistry*, 1990, **29**, 9799-9807.

2 X.-F. Huang, X. Lu, Y. Zhang, G. Q. Song, Q. L. He, Q. S. Li, X. H. Yang, Y. Wei and H. L. Zhu, *Bioorg. Med. Chem.*, 2012, **20**, 4895-4900.

3 N. Kapuriya, K. Kapuriya, X. Zhang, T.C. Chou, R. Kakadiya, Y. T. Wu, T. H. Tsai, Y. T. Chen, T. C. Lee, and A. Shah, *Bioorg. Med. Chem.*, 2008, **16**, 5413-5423.

4 L. Zhang, P. Zhan, X. Chen, Z. Li, Z. Xie, T. Zhao, H. Liu, E. De Clercq, and C. Pannecouque, J. Balzarini, *Bioorg. Med. Chem.*, 2014, **22**, 633-642.

5 H. Nawaz, Z. Akhter, S. Yameen, H.M. Siddiqi, B. Mirza and A. Rifat, *J. Organomet. Chem.*, 2009, **694**, 2198-2203.

6 M. Gizdavic-Nikolaidis, J. Travas-Sejdic, P. Kilmartin, G. Bowmaker and R. Cooney, *Curr. Appl. Phys.*, 2004, **4**, 343-346.

7 J.P. Silva, V.A. Machado, R.C. Calhelha, M.-J.R. Queiroz and O.P. Coutinho, *Drug Discov Ther.*, 2010, **4**, 246-256.

8 F.D. Suvire, M. Sortino, V.V. Kouznetsov, L.Y. Vargas M, S.A. Zacchino, U.M. Cruz and R.D. Enriz, *Bioorg. Med. Chem.*, 2006, **14**, 1851-1862.

9 I. Yilmaz, C. Kazak, S. Gümüş, E. Ağar and Y. Ardali, *Spectrochim Acta.*, 2012, **97**, 423-428.

10 J. Yao, Z. He, J. Chen, W. Sun, H. Fang and W. Xu, *Bioorg. Med. Chem. Lett.*, 2012, **22**, 6549-6553.

11 L.Y. Vargas M, M.a.V. Castelli, V.V. Kouznetsov, J.M. Urbina G, S.N. López, M. Sortino, R.D. Enriz, J.C. Ribas and S. Zacchino, *Bioorg. Med. Chem.*, 2003, **11**, 1531-1550.

12 V.V. Kouznetsov, L.Y. Vargas Méndez, M. Sortino, Y. Vásquez, M.P. Gupta, M. Freile, R.D. Enriz and S.A. Zacchino, *Bioorg. Med. Chem*., 2008, **16**, 794-809.

13 S.Y. Abbas, M.A. El-Sharief, W.M. Basyouni, I.M. Fakhr and E.W. El-Gammal, *Eur. J. Med. Chem*., 2013, **64**, 111-120.

14 E. Bendary, R. Francis, H. Ali, M. Sarwat and S. El Hady, *Annals. Agric. Sci*., 2013, **58**, 173-181.

15 L. Zhang, Q. Lang and Z. Shi, *Am. J. Anal. Chem*., 2010, **1**, 102-112.

16 J. Yano and S. Yamasaki, *Synthetic Metals*, 1999, **102**, 1157-1157.

17 X. H. Cai, K. Kalcher, C. Neuhold and B. Ogorevc, *Talanta*, 1994, **41**, 407-413.

18 S. Mu, *Biosensors and Bioelectronics*, 2006, **21**, 1237–1243.

19 A. Can, I. Yildiz and G. Guvendik, *Environ Toxicol Pharmacol*., 2013, **35**, 369-379.

20 A.B. Hill, P.R. Jefferies, G.B. Quistad and J.E. Casida, *Mutat Res Genet Toxicol Environ Mutagen*., 1997, **395**, 159-171.

21 F.E. Dayan and M.L.D.M. Zaccaro, *Pest Biochem Physiol*., 2012, **102**,189-197.

22 K.S. Ryu, K.M. Kim, Y.-S. Hong, Y.J. Park and S.H. Chang, *Bull. Korean Chem. Soc*., 2002, **23**, 1144-1148.

23 M. Angelopoulos, *IBM J Res Dev*., 2001, **45**, 57-75.

24 P.R. Somani and S. Radhakrishnan, *Mater Chem Phys*., 2003, **77**, 117-133.

25 M. Angelopoulos, N. Patel, J.M. Shaw, N.C. Labianca and S.A. Rishton, *J. Vac. Sci. Technol B*., 1993, **11**, 2794-2797.

26 K.R. Raghavendra and K. Ajay Kumar, *Int. J. ChemTech Res*., 2015, **5**, 1756-1760.

27 A. Shah, A. Ullah, A. Rauf, Z.U. Rehman, S. Shujah, S.M. Shah and A. Waseem, *J. Electrochem. Soc*., 2013, **160**, H597-H603.

28 I. Ullah, A. Naveed, A. Shah, A. Badshah, G.S. Khan and A. Nadeem, *J Surfactants Deterg*., 2014, **17**, 243-251.

29 A.J. Bard and L.R. Faulkner, Electrochemical Methods: Fundamentals and Applications, Wiley, 2001.

30 J. Wang, Analytical electrochemistry, John Wiley & Sons, 2006.

31 S.A. Ali and M. Sami, *Pak. J. Pharm. Sci.*, 2005, **18**, 6-17.

32 S. Munir, A. Shah, A. Rauf, A. Badshah, S.K. Lunsford, H. Hussain and G.S. Khan, *Electrochim. Acta*, 2013, **88**, 858-864.

33 S.A. Yasin, *Portugaliae Electrochim Acta*, 2006, **24**, 23-36.

34 A.C. Michael and L. Borland, Electrochemical methods for neuroscience, CRC Press, 2007.

35 T.A. Enache and A.M. Oliveira-Brett, *J. Electroanal. Chem.*, 2011, **655**, 9-16.

36 O. Thomas and C. Burgess, UV-visible spectrophotometry of water and wastewater, Elsevier Science, 2007.

37 C.A. Hollingsworth, P.G. Seybold and C.M. Hadad, *Int J Quantum Chem.*, 2002, **90**, 1396-1403.

38 S. Altınöz and B. Uyar, *Analytical Methods*, 2013, **5**, 5709-5716.

39 K. Ahmad, A.H. Shah, B. Adhikari, U.A. Rana, C. Vijayaratnam, N. Muhammad, S. Shujah, A. Rauf, H. Hussain and A. Badshah, *RSC Adv.*, 2014, **4**, 31657-31665.

40 R.M. Kotkar and A.K. Srivastava, *Sensor Actuat B Chem.*, 2006, **119**, 524-530.

41 J. Liu, L. Cheng, B. Liu and S. Dong, *Langmuir*, 2000, **16**, 7471-7476.

42 A. Zaouak, F. Matoussi and M. Dachraoui, *Int. J. Electrochem.*, 2011, **2011**, ID 904570, 1-6.

43 M. S. Zakerhamidi, A. ghanadzadeh and M. Moghadam, *Chem. Sci. Trans.*, 2012, **1**, 1-8.

44 M. S. Masoud, A. E. Ali, M. A. Shaker and M. A. Ghani, *Spectrochim. Acta*, 2004, **60**, 3155-3159.

Schemes

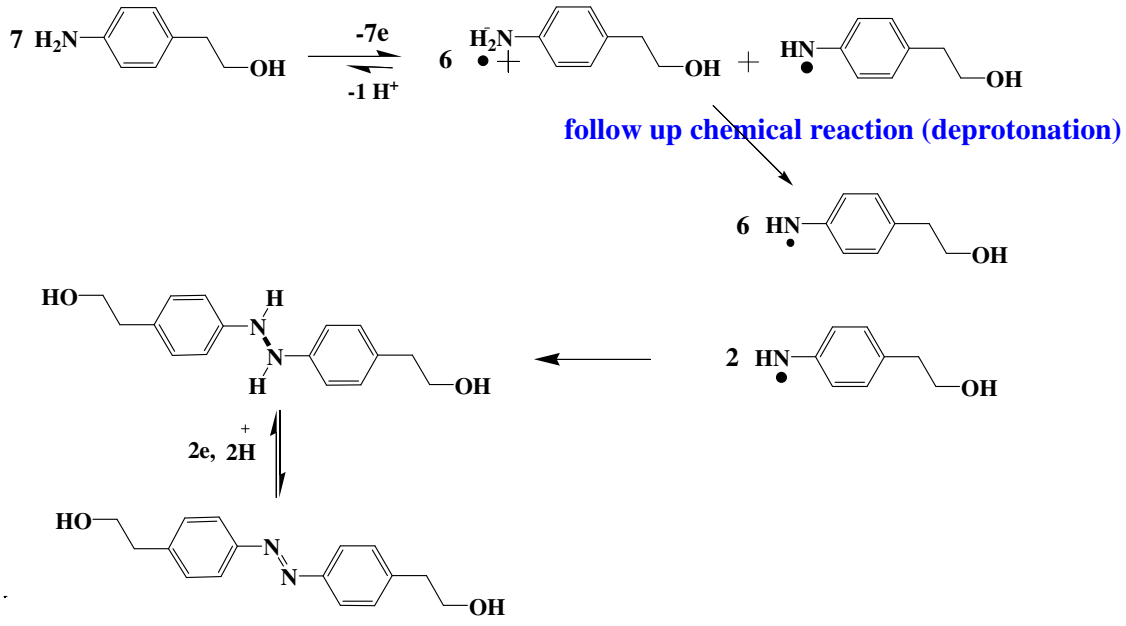

Scheme 1. Proposed oxidation mechanism of 4-APA in solutions of pH ≤ 6.

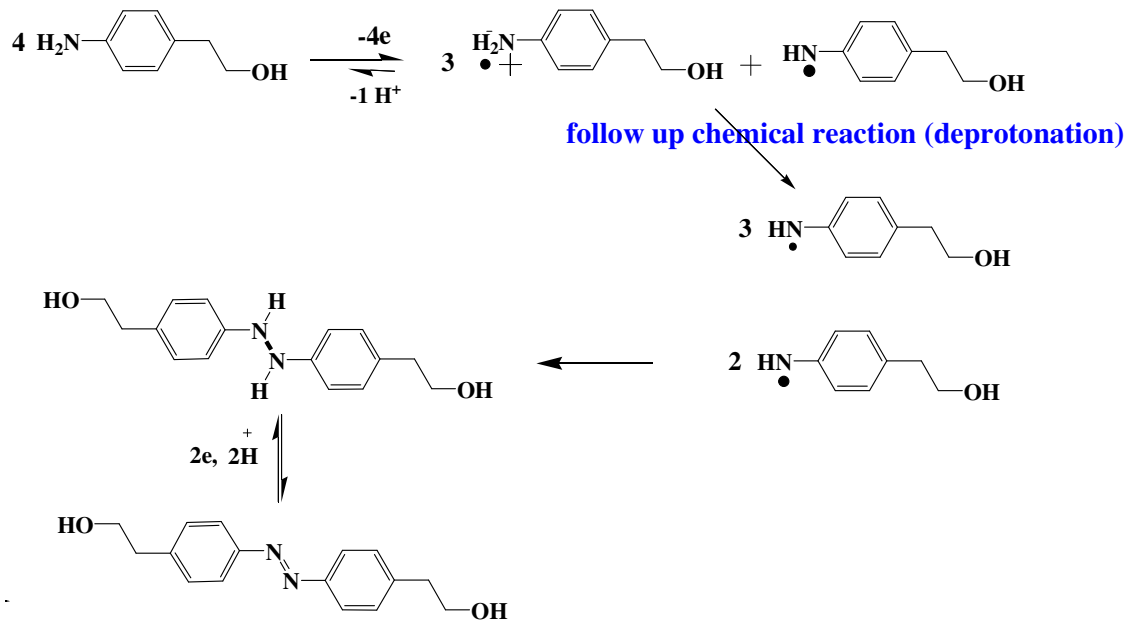

Scheme 2. Proposed oxidation mechanism of 4-APA in media of pH > 6.

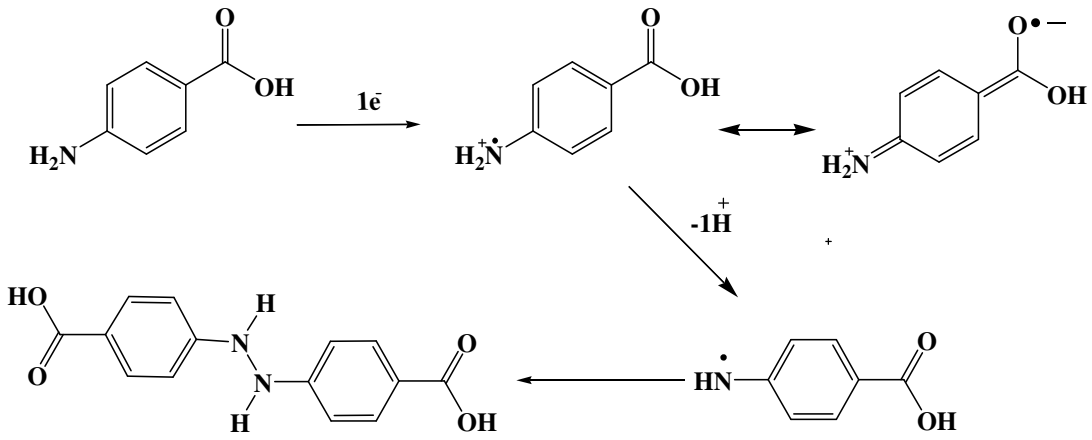

Scheme 3. Proposed oxidation mechanism of 4-ABA corresponding to peak 1a.

Tables

Table 1. Diffusion coefficient and heterogeneous rate constant values for 4-APA and 4-ABA calculated at different temperatures.

Compounds	Temperature/K	$\alpha_a n$	$D/10^{-5}$ cm^2 s^{-1}	$k/10^{-3}$cm s^{-1}
4-APA	308	0.40	5.20	3.33
	313	0.45	5.39	3.43
	318	0.51	5.63	3.76
	323	0.55	5.88	4.12
	328	0.62	6.35	4.52
4-ABA	303	0.43	4.75	3.24
	308	0.49	4.97	3.44
	313	0.54	5.31	3.83
	318	0.57	5.52	4.26
	323	0.61	6.07	4.48
	328	0.63	6.56	4.83

Table 2. Thermodynamic parameters of aniline derivatives as determined from CV

Comp.	Temperature/K	$\Delta G^{\#}$/(kJ/mol)	Ea/(kJ/mol)	$\Delta H^{\#}$/(kJ/mol)	$\Delta S^{\#}$/(J/K.mol)
4-APA	308	43.77	13.69	11.13	-12.75
	313	43.69		11.09	-12.53
	318	43.46		11.05	-12.26
	323	43.24		11.00	-12.00
	328	43.00		10.97	-11.75
4-ABA	303	43.84	13.78	11.26	-12.93
	308	43.69		11.22	-12.68
	313	43.42		11.17	-12.39
	318	43.15		11.13	-12.11
	323	43.02		11.09	-11.89
	328	42.83		11.05	-11.66

Table 3. Number of electrons, protons and pKa of aniline derivatives calculated from DPV

Compounds	Peaks	No. of electrons	Slope E_p-pH plot (V/pH)	No. of protons	PKa
4-APA	1a	1	-0.020	0.14	6.0
			-0.035	0.25	
	2a	1	-0.083	1	
	3a	1	-0.090	1	
4-ABA	1a	1	-0.043	0.30	7.9
	2a	1	---	1	
	1c	1	---	1	

Table 4. LOD and LOQ of aniline derivatives and other linear fit parameters calculated from calibration curves.

Compounds	SD /10^{-7} (A)	Slope/10^{-5} ($Adm^3(\mu mol)^{-1}$)	LOD/ ($\mu molL^{-1}$)	LOQ/ ($\mu molL^{-1}$)	Linearity range (μM)
4-APA	2.469	6.128	12.09	40.29	7.5-80
4-ABA	2.468	6.127	12.08	40.29	30-479

Table 5. Computationally determined parameters of aniline derivatives

Parameters	4-APA	4-ABA
E_{HOMO} / (e V)	-5.269	-5.974
E_{LUMO} / (e V)	0.0591	-1.083
I.E / (e V)	5.269	5.974
E.A / (e V)	0.059	0.040
Oxidation potential / (V)	0.725	0.863
Dipole moment / (Debye)	3.788	8.028

Figures

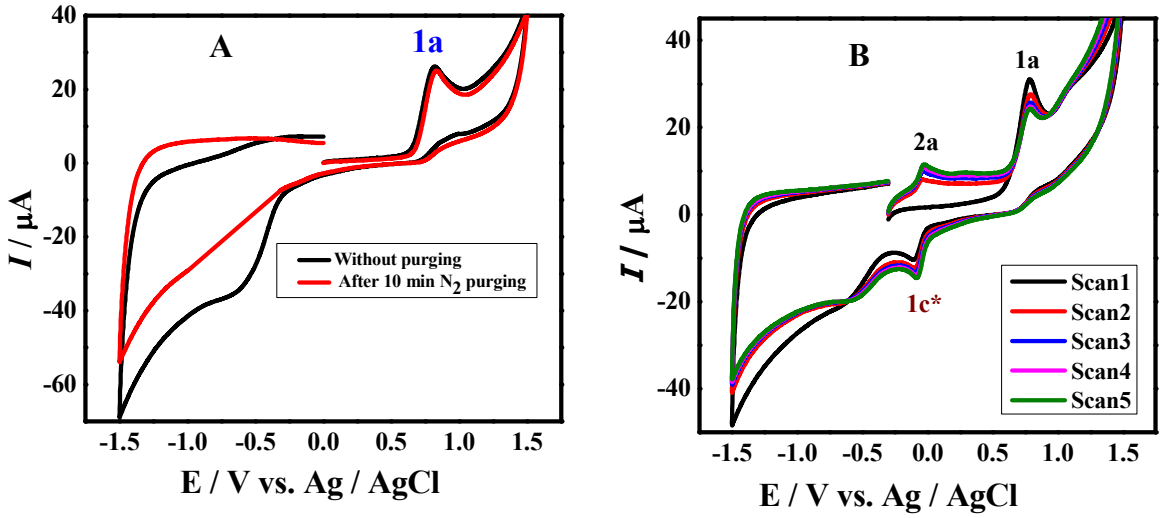

Fig. 1. CVs of 1mM (A) 4-APA and (B) 4-ABA obtained in a medium of pH 7.4 at a scan rate of 100 mVs^{-1}.

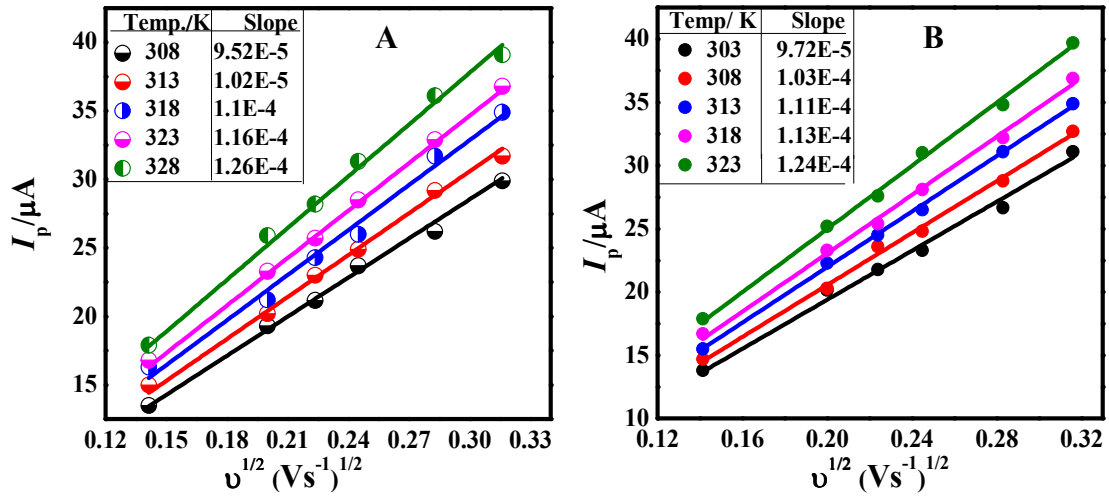

Fig. 2. Plots of current intensity of peak 1a *versus* square root of scan rate using 1mM solution of (A) 4-APA and (B) 4-ABA.

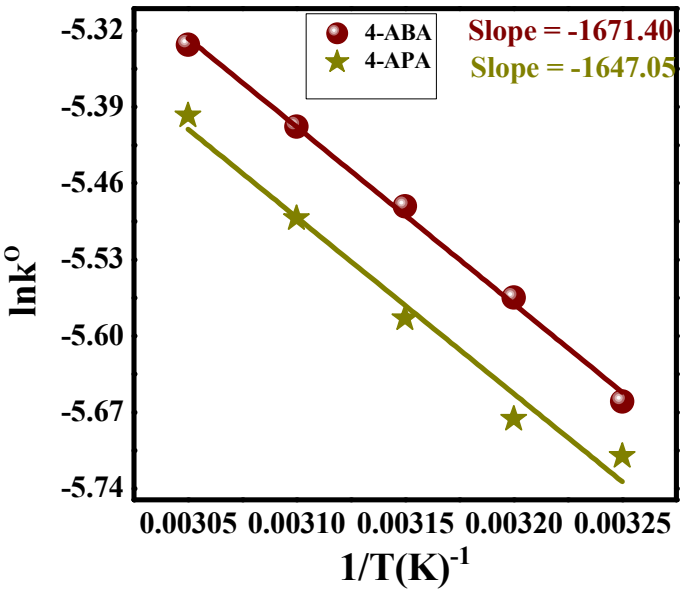

Fig. 3. Plots of $\ln k^{o}$ as a function of 1/T.

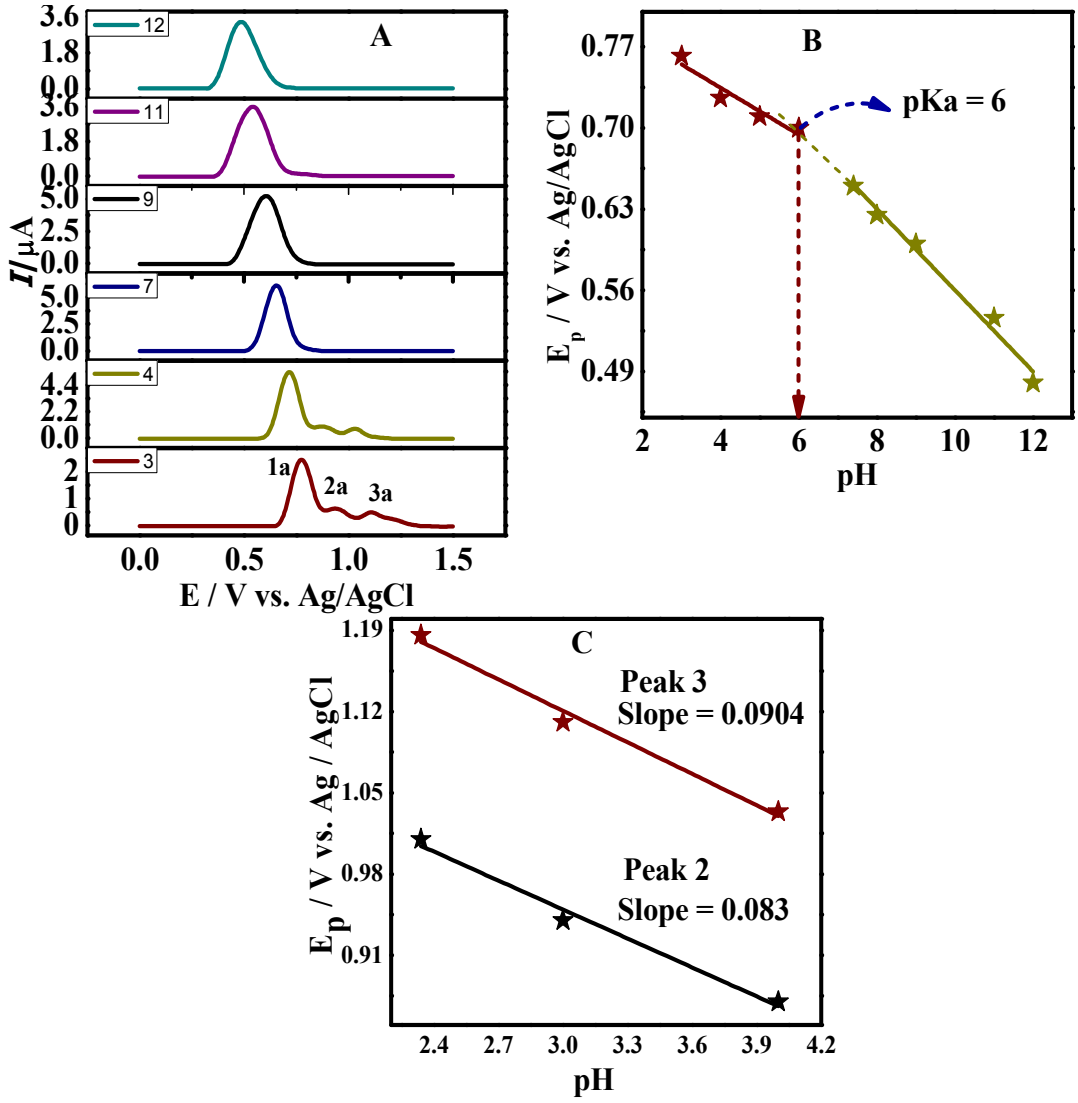

Fig. 4. (A) DPVs of 4-APA recorded in in the pH range 3 - 11at 5 mVs^{-1}. E_p - pH plots of 4-APA corresponding to peak (B) 1a (C) 2a and 3a.

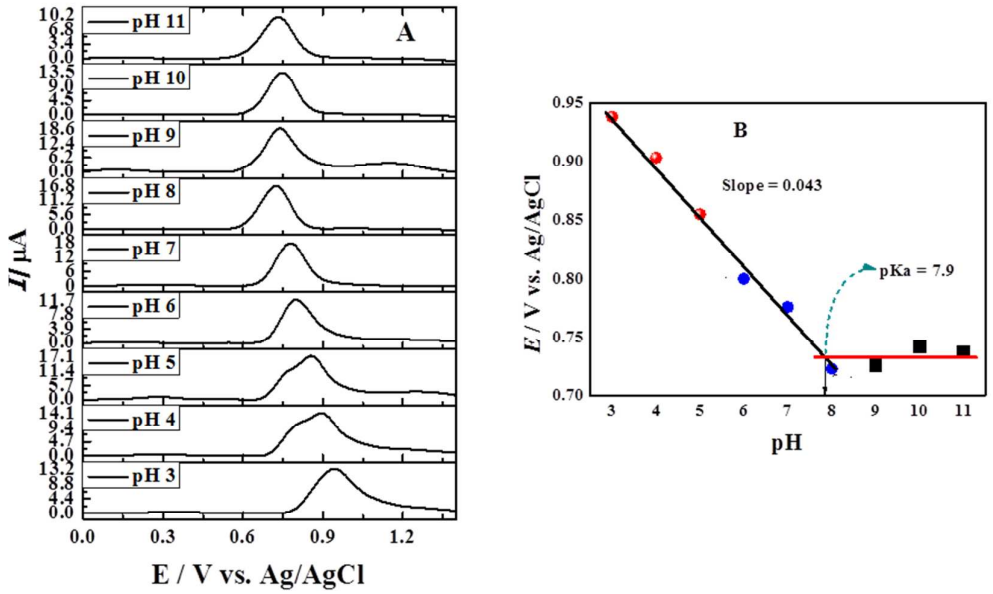

Fig. 5. (A) DPVs of 4-ABA obtained in the pH range 3 - 11at 5 mVs^{-1} and (B) Plot of peak potential as a function of pH.

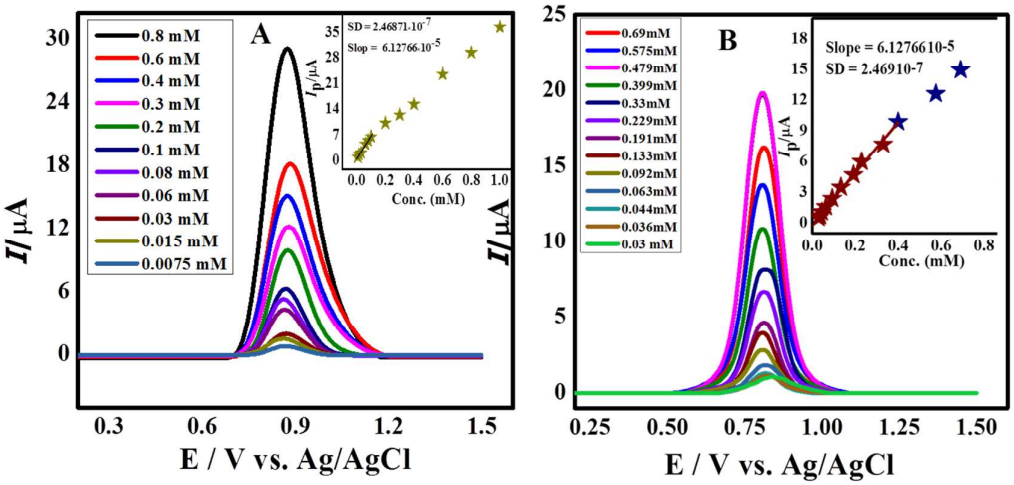

Fig. 6. SWVs of different concentrations of (A) 4-APA and (B) 4-ABA obtained at 100 mV s^{-1} in a medium of pH 7.4. Insets show current intensity vs. concentration plots.

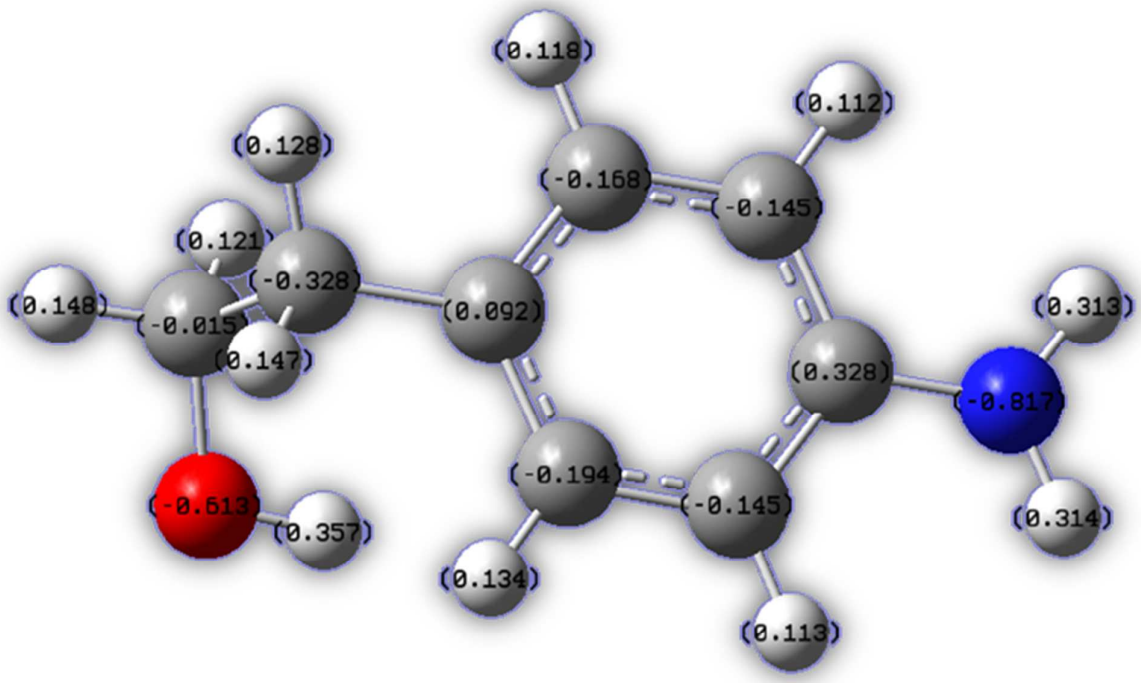

Fig. 7. Mullikan charge distribution on atoms of 4-APA.

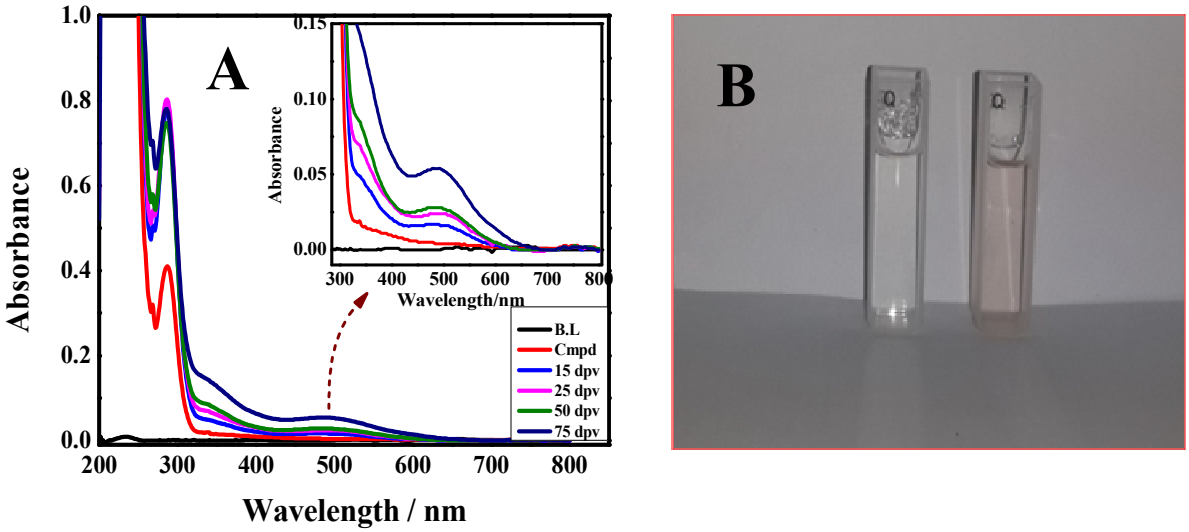

Fig. 8. (A) UV-Vis spectra of 4-APA recorded after different number of DPV scans, inset spectra is a demonstration of better visualization of signal around 485 nm (B) Colorless solution of 4-APA and light red colored solution of its oxidized product obtained from the electrode surface after 75 scans.